Screening and Surface States in Molecular Monolayers Adsorbed on Silicon

Fabrizio Cleri,*,†,‡ Sara Letardi,† and Christophe Delerue‡

Institut d'Electronique, Microélectronique et Nanotechnologie, Av. Poincaré B.P. 60069, Villeneuve d'Ascq Cedex F-59652, France, and Ente Nuove Tecnologie, Energia e Ambiente, Centro Ricerche Casaccia, C.P. 2400, I-00100 Roma A.D., Italy

Received: September 22, 2005; In Final Form: April 3, 2006

We performed density functional theory calculations of the atomic and electronic structure of a dense monolayer of phenyl-terminated alkyl chains chemisorbed onto the (100) Si surface. Different adsorption sites were characterized for both the pristine and (2 × 1) reconstructed surface. A strong effect on the ordering and alignment of the molecular energy levels with respect to the Fermi level of silicon is observed, consequent to intermolecular screening in the monolayer and of the appearance of surface localized states, as a function of the different bonding arrangements. Some possible consequences of these findings are discussed in the framework of the experimental synthesis of such monolayers as molecular current rectifiers in silicon-integrated nanoscale electronics.

1. Introduction

Molecular electronics, aimed at reproducing at the molecular scale all the basic functionalities of conventional, silicon-based microelectronics, such as commutation, data storage, interconnection of a large number of logical gates, and memory elements, over distances of 1−10 nm, is one of the most promising directions in nanotechnology.[1] The building blocks of future molecular electronics devices could be specially designed organic molecules assembled on appropriate substrates into useful circuits through the processes of self-assembly, i.e., the spontaneous organization of the molecular building blocks.[2] This process is governed by the formation of both covalent and noncovalent bonds, e.g., hydrogen bonds and dispersion forces (van der Waals), both within the molecules and with the substrate surface. The type of bonding to the surface may affect the final electronic characteristics of the sought device because the atomic-scale details of the interface are at the origin of the contact resistance and, moreover, influence the quantum transport properties. Therefore, understanding the intermolecular bonding and the interactions with surfaces is crucial for the appropriate choice of the molecular and substrate material for nanostructure design.

From the experimental point of view, the direct observation of the molecular self-assembly at surfaces has became possible with the introduction of the scanning tunneling microscope (STM). On the theoretical side, the increasing computer power and the development of new computational techniques allow prediction directly from the fundamental quantum mechanical laws the preferential geometry of the molecular arrangements as well as the strength and the nature of the chemical bonds involved. Unfortunately, such a degree of theoretical accuracy is restricted to the study of systems of very small sizes, whereas the statistical properties of extended molecular aggregates over large surfaces, at finite temperature and pressure, can be extracted only from more approximate molecular dynamics simulations with empirical force fields. The combination of such theoretical and computational tools can give a deeper insight into the chemistry and physics of the self-organization process.

Self-assembled monolayers (SAM) on solid substrates, which have been studied for a long time in the context of organic semiconductors,[3] have a great potentiality also as nanoelectronic devices, especially in view of their incorporation into conventional, silicon-based microelectronics. Indeed, densely packed SAMs of all-trans extended alkyl chains are known to act as insulating layers on Si surfaces.[4] Moreover, attaching different types of functional endgroups to the free end of the alkyl chains can give rise to molecular junctions of different types, as demonstrated in recent experiments.[5] For example, a termination of the insulating, alkyl σ chain with a phenyl or thiophene π-conjugated head, could give rise to a molecular rectifying p−n junction.

In this work, we study, by means of density functional theory (DFT) electronic structure calculations, the chemical bonding and electronic properties of a dense monolayer of a model $\sigma-\pi$ molecule chemisorbed on the Si(100) surface. Previous calculations of the interaction of small hydrocarbon molecules with reconstructed Si surfaces have been performed, by using all-electron cluster methods, or by DFT with a periodic supercell, on very small model systems.[6−8] Here, we exploit the full potential of the plane-wave expansion in a periodic computational supercell to simulate the formation of extended, multilayered, organic/inorganic semiconductor interfacial structures. Within the bounds of the capabilities offered by modern DFT numerical techniques, based in our case on the local-density approximation and on the pseudopotential theory to represent the core electrons, by such simulations we are able elucidate specific features of the assembly of Si−monolayer systems that have an impact on the final performances of the nanoelectronic device. The paper is organized as follows. In Section 2, the problem of electrostatic screening in a dense molecular monolayer is addressed, showing how it affects the molecular energy levels in the neighborhood of the conduction gap. In Section 3, we verify our computational model against some well-known, and less known, facts about the chemistry of hydrogen on the

* Corresponding author. E-mail: fabrizio.cleri@iemn.univ-lille1.fr.
† Ente Nuove Tecnologie, Energia e Ambiente, Roma, Italy.
‡ Institut d'Electronique, Microelectronique et Nanotechnologies, Villeneuve d'Ascq, France.

10.1021/jp055395t CCC: $33.50
Published on Web 05/18/2006

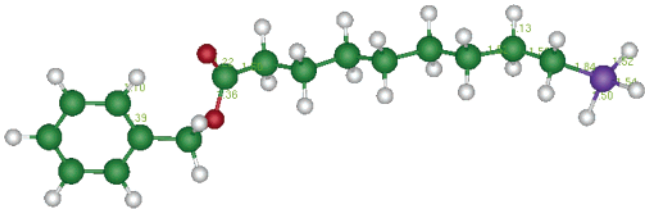

Figure 1. Schematic ball-and-stick representation of the SNP molecule. H atoms are the smaller, light-grey balls. O atoms are the medium-sized, dark-grey balls.

Si(100) surface. Then, in Section 4, we discuss different bonding configurations of the Si−monolayer interface with respect to their relative chemical stability, atomic structure, and electronic properties. Finally, in Section 5, we draw some conclusions of our study. A summary of the computational details is also given at the end of the paper.

2. Coulomb Screening in the Monolayer

The SAM system studied by means of computer simulation in the present work is based on the $H_3Si(CH_2)_8COO-H_2C$(1,phenyl) molecule (or 9-silyl-nonyl phenyl-acetate, shortly called SNP), arranged in a dense monolayer, contacted to a Si(100) substrate via the silane foot. We chose to model a SiH_3-terminated molecule on a clean Si surface for the sake of computational simplicity. However, it should be noted that, in real SAM synthesis, Si surfaces are usually covered by a layer of native oxide, and the alkyl chains are terminated by $-SiCl_3$ to allow chemisorption.[5,9]

The atomic structure of the free SNP molecule is shown in Figure 1. After structural relaxation, we find that all the typical bond lengths, C═C, C−C, C−H, and C−O, are within the experimental values. The silane termination has the following bond lengths: C−Si = 1.84 Å and Si−H = 1.52 ± 0.02 Å. The level spectrum displays a HOMO−LUMO gap of $\Delta = 4.62$ eV. We find a negative value for the electron affinity: $A = E(N+1) - E(N) = -1.02$ eV, while the ionization energy is: $I = E(N-1) - E(N) = +6.83$ eV, where $N = 102$ is the number of valence electrons in the system. Therefore, the "conductivity gap" is $I-A = 7.86$ eV. By the LDOS analysis, we have that the HOMO and LUMO levels are entirely localized on the head of the molecule, the LUMO bearing a stronger π character from the phenyl, while the HOMO is partly localized on the double-oxygen bridge. Notwithstanding the numerical error of the LDA approximation, we note that the experimentally measured electron affinity for gas-phase benzene and other phenyl-based and polyaromatic molecules is, indeed, found to be negative.[10]

To quantify the role of intermolecular interactions, the electronic structure of the SNP molecule was calculated also in a dense two-dimensional monolayer with the same density and geometrical arrangement it would take on the Si(100) surface. The molecule, with its major axis approximately parallel to the Z direction, was then adjusted to fit in a periodic box of XY area of $5.4050 \times 5.4050 = 29.21$ Å^2, with free top and bottom surfaces along Z (Figure 2). Such an (inverse) density is only slightly larger and very close to the maximum XY packing attainable for the SNP molecule, as obtained from a separate cell-minimization calculation of the monolayer in the XY plane, which gave a square lattice of $5.3904 \times 5.3875 = 29.04$ Å^2. Moreover, such a density is in good agreement with the typical packing density of polyalkyl chains experimentally observed on various substrates or condensed in solution. It is worth noting that the minimum distance between two H atoms in two nearby molecules is around 3 Å, so that there is no possibility of covalent cross-linking between adjacent molecules in the monolayer.

The total energy is lowered by the intermolecular interactions by $\Delta E = -2.21$ eV/molecule with respect to the free molecule, or $\Delta E_S = -1.21$ J/cm^2 in terms of the specific surface of the monolayer. This seems a reasonable figure when considering that the average length of the molecule in the Z direction is about 19 Å; therefore, the relative dispersion force is of the order of 0.1 eV/Å (although it is well-known that van der Waals forces are poorly estimated by DFT calculations). Such a small interaction energy should lead to a relatively small width of the energy bands in the dense monolayer, also because of the 2D arrangement. For the sake of comparison, in a DFT-GGA simulation of a dense 3D slab of benzene molecules with free surfaces,[11] a HOMO−LUMO gap of 4.4 eV and a bandwidth of 0.70−0.72 eV for the HOMO-1, HOMO, and LUMO bands was obtained.

The molecular energy level spectra of the free molecule and of the monolayer are compared in Figure 2b. The monolayer HOMO−LUMO gap is $\Delta = 4.46$ eV, i.e., slightly smaller than the 4.62 eV found for the free molecule. However, not only the whole level spectrum is almost rigidly blue-shifted to more positive energies, but the energy levels are substantially rearranged as far ar their relative spacing and the angular-momentum character. From the LDOS analysis, the HOMO still appears strongly localized on the headgroup, with a strong π character as for the free molecule. A small mixing of σ states appears in the LUMO compared to the free molecule, which is a possible explanation for the reduction of the HOMO−LUMO gap by ∼0.12 eV. Incidentally, we note that a rigid shift is frequently observed experimentally.[12] However, those experiments look at photoemission spectra of molecular films and, thus, at states of the molecular ion. In that case, shifts between gas-phase and condensed-phase molecules measured by photoemission are due to polarization/screening induced by the photogenerated hole. Such an effect is unrelated to our case because we are studying the neutral molecule.

The calculation of the ionization potential, I, for a molecule embedded in a monolayer reveals that, because of the formation of extended molecular states, the ionization process does not affect a single, well-defined electron level. Rather, several orbitals in a narrow band around the HOMO are fractionally affected by electron removal. In other words, this can be interpreted as a strong screening of the Coulomb field of the pointlike dipole in the molecular monolayer. In this respect, it should be noted that, as the intermolecular distance is reduced, the pointlike charge approximation fails and the full multipolar anisotropy of the polarizability tensor, with terms decaying much faster than $1/r$, becomes relevant.[13] For the SNP, we obtained a value of $I = +4.60$ eV, to be compared to the above $I = +6.83$ eV for the free molecule.

The intermolecular screening obviously affects also the conductivity gap. From the value of the electron affinity calculated for the SNP dense monolayer, $A = +0.64$, the conductivity gap is: $I-A = 3.96$ eV, i.e., it is reduced by about a factor of 2 with respect to the value of 7.86 eV for the free molecule.

To estimate the possible role of thermal disorder on intermolecular screening, we performed an auxiliary set of calculations on a (3×3) slab of the smaller molecule toluene ($CH_3C_6H_5$), with the same densely packed arrangement of the SNP molecule (similar to Figure 2a), or with some thermal disorder added to the configuration. Note that such a smaller

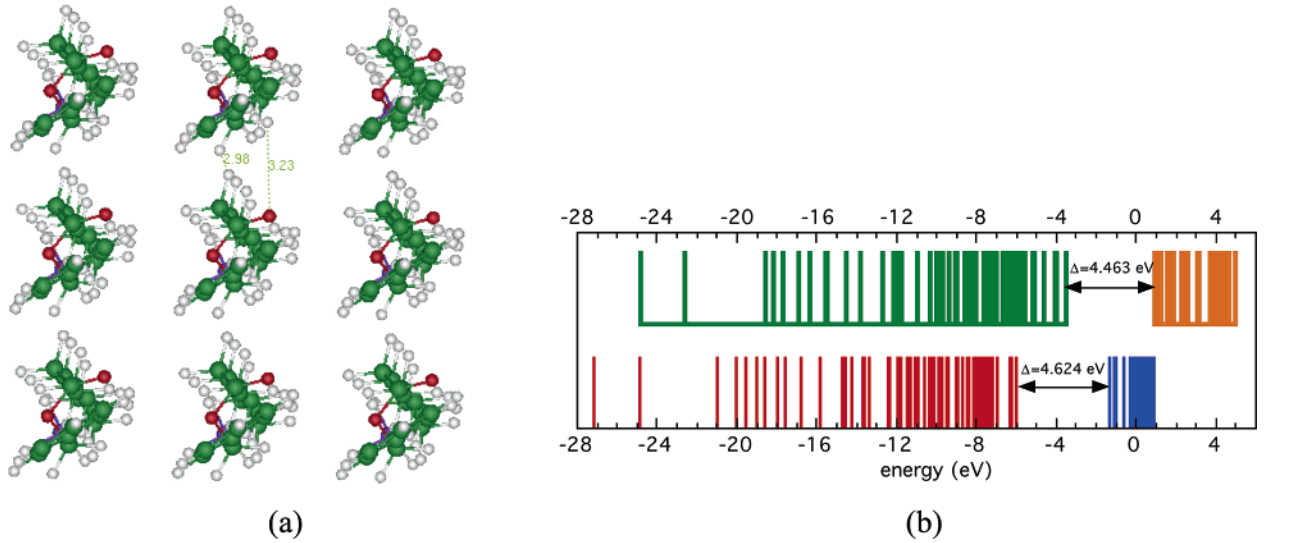

Figure 2. (a) *XY*-plane projection of the periodically repeated unit cell for the simulation of a free-standing dense monolayer of the SNP molecule. (b) Comparison of the energy level spectrum for the free molecule (bottom row) and the dense monolayer (top row).

molecule, indeed, represents just the terminal head of the SNP, which is largely responsible for the electronic structure around the HOMO−LUMO gap. For the free toluene molecule in the gas-phase, we obtained $I = +7.41$ eV. However, when nine toluene molecules are regularly packed in a box at the same density as the SNP above, the ionization potential reduces to $I = +4.36$ eV, showing a quantitatively similar screening effect. Moreover, we find that thermal disordering is not enough to destroy such a screening effect because, for the disordered nine-molecule configuration, we obtain a comparable value, $I = +4.29$ eV.

Despite the approximations usually made in computing long-range electrostatic interactions in a periodic system,[14] it is worth noting that such a quenching of the ionization potential is qualitatively similar in all the phenyl-based systems examined, meaning that the largest effect of the molecular packing is the electrostatic intermolecular screening. In the simple Hubbard picture, in which the quantity $U = I - A$ has the meaning of an on-site Coulomb repulsion, mutual screening between a charge and its image at a distance d would shift A and I by equal and opposite amounts, $\pm e^2/4d$, thereby reducing U down to $U - e^2/2d$. In our case (see Figure 2b), such a (almost) symmetric shift can be inferred by scaling the values of I and A to the HOMO−LUMO mid-value, $E_{HL} = -3.55$ and -2.26 eV for the free molecule and for the monolayer, respectively. Indeed, we find that A is decreased by 0.90 eV, while I increases by 0.94 eV. Overall, the conductivity gap is reduced down to becoming very close to the HOMO−LUMO gap, thus indicating that the on-site repulsion is almost completely screened in the monolayer. Such a strong polarization screening behavior has been reported also for other systems, such as C60 monolayers, and poly-phenyl-vinylene oligomers on Ag and Au.[12,15−17]

3. Hydrogen Chemistry of the Si(100) Surface

For our subsequent Si−monolayer interface calculations, we built a Si(100) periodic surface slab with a (2 × 2) planar unit cell in *XY* and lattice parameter $a_0 = 5.4050$ Å, made up of eight layers along Z ($L_z = 10.81$ Å). For the sake of comparison, a longer supercell containing 12 layers of Si along Z ($L_z = 16.215$ Å) was also used in some calculations. The bottom-surface dangling bonds are saturated with H, and this hydrogen layer together with the lowermost 2−4 Si layers were held frozen during all the foregoing structure relaxation calculations.

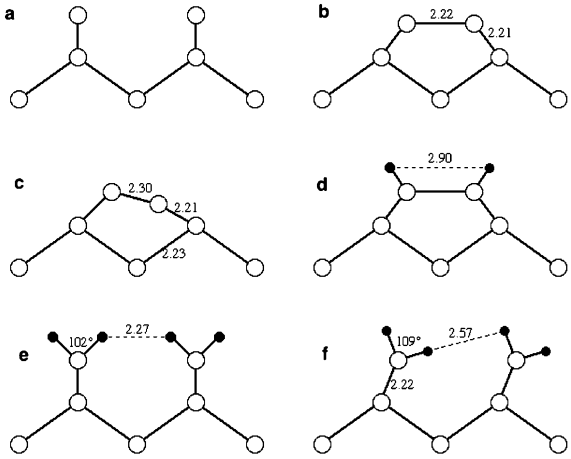

Figure 3. Configurations of the Si(100) surface. (a) (1 × 1) unreconstructed, (b) (2 × 1) dimerized, (c) (2 × 1) broken-symmetry, (d) (2 × 1) monohydride, (e) (1 × 1) dihydride, and (f) (1 × 1) tilted dihydride. Bond lengths are in Ångstroms.

The Si(100) surface is well-known to undergo a (2 × 1) dimer reconstruction in which, moreover, the symmetry in the perpendicular direction should be broken by a Jahn−Teller distortion,[18,19] the dimer becoming buckled (Figure 3). Other possible reconstructions have been proposed such as a (2 × 2) or a (4 × 2).[20] To verify the quality of our DFT-LDA pseudopotential model, we calculated the relaxed structures for the unreconstructed (Figure 3a), (2 × 1) dimerized (Figure 3b), and (2 × 1) broken-symmetry (Figure 3c) variants, finding good agreement with previous theoretical results. In particular, the energy of the (2 × 1) dimerized is lower than that of the unreconstructed surface by 2.68 eV/surface unit (or 1.34 eV/dangling bond), in quite good agreement with the literature data,[18−20] when considering that we are using the LDA approximation. The Jahn−Teller distortion further lowers the energy by 0.40 eV/surface unit. The changes in the most relevant bond lengths are also displayed in Figure 3. It is worth noting that the presence of dangling bonds makes the surface metallic; therefore, convergence of our DFT calculations could be obtained only with a Fermi−Dirac smearing of the occupation numbers, with a width of 0.005 Ha. However, it should be noted that more refined GW calculations[21] showed that buckling of

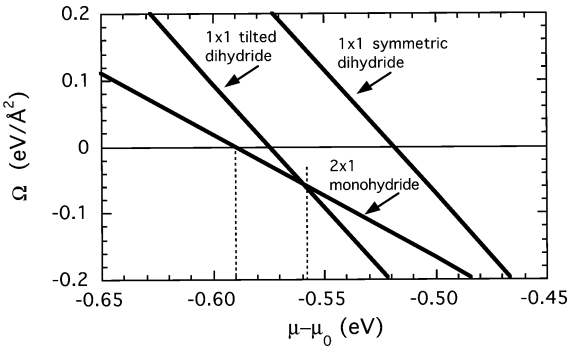

Figure 4. Grand-canonical potential per unit surface area as a function of the H chemical potential, μ_H, for the (2 × 1) monohydride and two variants of the (1 × 1) dihydride Si(100) surface. The origin of the H chemical potential is scaled to the reference state μ_0 (see text).

the dimer reopens the semiconductor gap (the underestimation of the gap being a well-known pitfall of the LDA).

The hydrogenation of the Si(100) surface is readily studied experimentally by exposure of the clean surface to atomic H at substrate temperatures from ambient to $T \sim 300$ °C[22,23] (see again Figure 3). The most commonly observed phase is the (2 × 1) monohydride (Figure 3d) which, hovewer, is obtained at the higher substrate temperatures. At T close to room temperature, a (1 × 1) dihydride phase (Figure 3e,f) is observed, and less frequently, a (3 × 1) phase, which results from the symmetrical alternation of (2 × 1) and (1 × 1) surface rows.

We calculated the relaxed structures also for hydrogenated surfaces because they will appear in the following Si−monolayer interface systems. Because the surface variants have different H stoichiometry, to compare their relative stability, one must calculate the total grand-canonical potential, Ω, i.e., including also the H chemical potential, μ_H, and the difference in the vibrational entropy, ΔS, of the initial and final states, as:

$$\Omega = E_{TOT} - E_{clean} - n_H(\mu_H - \mu_0) - \mu_{Si(bulk)} - T\Delta S \quad (1)$$

where E_{TOT} is the total energy of the surface with n_H H atoms, E_{clean} is the lowest-energy clean surface, i.e., the broken-symmetry dimer reconstruction (Figure 3c), and μ_0 is the chemical potential of a reference state, eventually including the zero-point energy of the (free) H atoms. At $T = 0$, the entropy contribution will vanish. Although the actual value of μ_0 is not relevant to our results, a suitable reference state could be, e.g., the H pressure at which SiH_4 is formed spontaneously from atomic H and bulk Si, $\mu_0 = [E(SiH_4) - \mu_{Si(bulk)}]/4$.

The calculated grand potential is shown in Figure 4 as a function of the H chemical potential. It can be noted that, up to a threshold value of $\mu_H = \mu_0 - 0.590$ eV, the clean surface is stable; then, in an interval of $\mu_H = \mu_0 - 0.590$ to $\mu_0 - 0.558$ eV, the (2 × 1) monohydride (see Figure 3d) is the stable phase; finally, at $\mu_H > \mu_0 - 0.558$ eV, the (1 × 1) tilted dihydride (Figure 3f) becomes stable. The tilted dihydride configuration is lower in energy by 0.22 eV with respect to the symmetric (1 × 1) dihydride (Figure 3e) because the H−H distances and angles are optimized in the former. Notably, for whatever value of μ_H, the symmetric (1 × 1) dihydride is never stable, in agreement with earlier findings.[24]

As far as the electronic structure is concerned, in Figure 5, we report the LDOS projected on the four topmost layers of the surface for the reconstructed configurations both clean and hydrogenated. In agreement with previous DFT calculations, we find that all the Si clean surfaces are metallic, including the broken-symmetry one (Figure 5b,c). However, despite the full

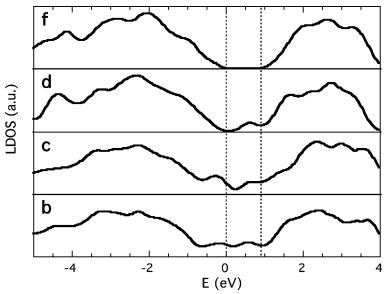

Figure 5. Localized density of states (LDOS) for the topmost 4 layers of the Si(100) surface in different reconstructed configurations (see also Figure 4). (b) (2 × 1) dimerized symmetric, (c) (2 × 1) broken-symmetry dimer, (d) (2 × 1) monohydride, (f) (1 × 1) tilted dihydride.

saturation of the surface dangling bonds, not all of the hydrogenated surfaces result clearly in semiconductors: while the tilted dihydride (Figure 5f) has a gap of 0.97 eV, the (2 × 1) monohydride (Figure 5d) displays a wide band of states that nearly fills the gap. Such states are only partly localized at the surface, being rather shared with the deeper atomic planes. We note that, in all the reconstructed surfaces, the "back" bonds pointing to the deeper planes are largely strained. Such distorted bonds could be an additional source of gap states, increasing the metallic character in the clean surfaces and tending to close the semiconductor gap in the (2 × 1), which can be seen as a partly reduced surface. Notably, a similar role of the back-bonds was recently suggested by scanning tunneling spectroscopy data of clean Si(100) surfaces in different reconstructions.[25]

4. The Si(100)−Monolayer Interface

A. Chemical Stability. Because the Si(100) displays a (2 × 1) reconstruction, we studied the chemisorption of the SNP molecule on such a surface in three different bonding configurations, whose fully relaxed configurations are represented in Figure 6 in a ball-and-stick model: (1) a single-bond configuration, in which the terminal silane group loses one H, binding to one surface Si atom, while the other Si is saturated by two H atoms (Figure 6a); (2) a single-bond configuration, in which the Si(100) surface undergoes a (1 × 2) reconstruction, and the SNP molecule binds to one of the dimerized surface Si atoms by losing one H atom from the terminal silane group, which likely saturates the other Si of the surface dimer (Figure 6b); (3) a double-bond configuration, with the Si(100) surface (1 × 2) reconstructed, and the SNP molecule bound to both the surface Si atoms in a "bridge" position by losing two H atoms from the terminal silane group (Figure 6c). The supercell for (1), (2), and (3) contained 63, 65, and 67 atoms, respectively. The corresponding chemical reactions can be schematically written as:

$$R{-}SiH_3 + Si(100) + 2H \leftrightarrow R{-}SiH_2@Si(100){:}2H \quad (1)$$

$$R{-}SiH_3 + Si(100) \leftrightarrow R{-}SiH_2@Si(100){:}H \quad (2)$$

$$R{-}SiH_3 + Si(100) \leftrightarrow R{-}SiH@Si(100) + 2H \quad (3)$$

where R represents the $(CH_2)_8COO\text{-}H_2C$(1,phenyl) portion of the SNP molecule, and Si(100) is the lowest-energy configuration of the clean surface, i.e., the broken-symmetry (2 × 1) dimer reconstruction.

Because each of the above reactions has a different H stoichiometry on the left and right sides, the relative probability depends on the pressure of free atomic H available. Under UHV conditions, i.e., for vanishing H supply from the outside, reaction

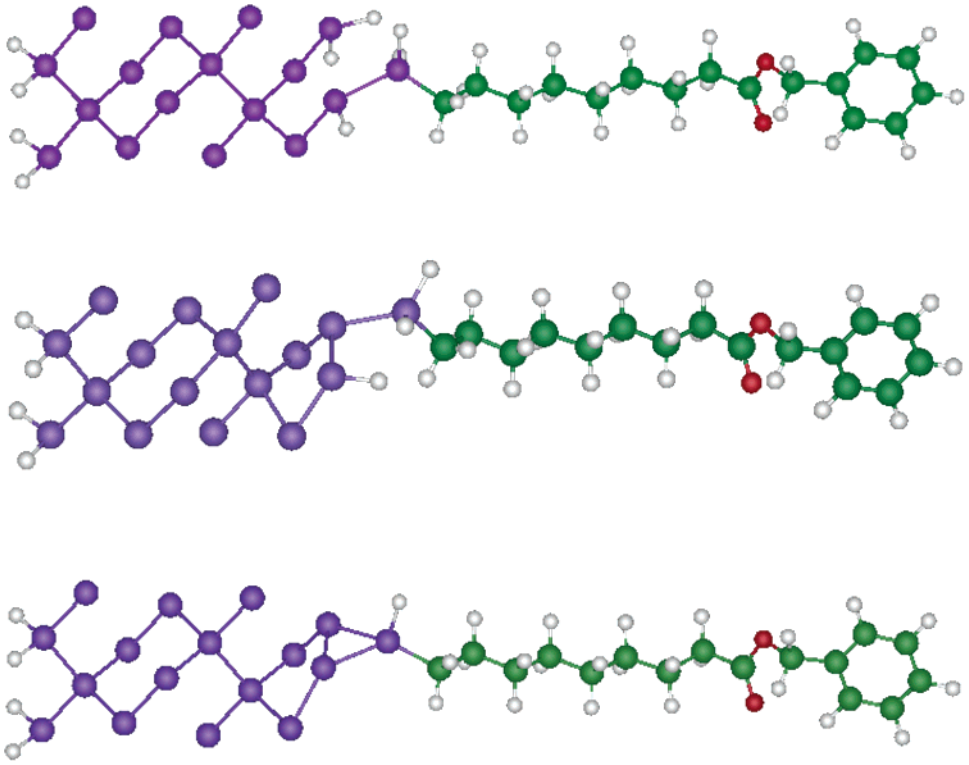

Figure 6. Ball-and-stick model of the relaxed atomic structures of the Si(100)−SNP monolayer interface, for the bonding configurations (1), (2), and (3) (see text).

2 will be initially favored. However, when statistically, reaction 3 should also occur, the H chemical potential would increase and also the (3) may become possible. The reaction 2 could go in the (1) by an intermediate state, e.g., a (2′) configuration in which the Si−Si dimer is cleaved, both surface Si atoms unsaturated by missing 1 H each, or a (2″) in which one Si is fully saturated and the other has two dangling bonds. Such intermediate configurations could be further stabilized by H addition, ultimately going into the (1).

For any bonding configuration, the simulated molecular system forms a dense organic monolayer covering the Si(100) surface. Such an effect is described by periodic boundary conditions in the *XY* plane, while along the (periodic) *Z* direction, a void of about 10 Å separates the top and bottom surfaces. As noted above, the *XY* packing is such that the molecules are well separated so as not to interact with each other by forming covalent bonds. Such a surface density (1/29.2 molecule/Å^2) is around the maximum expected for a "good" surface adsorbed monolayer (see, e.g., refs 26, 27 in which densities between 1/20 to 1/40 molecule/Å^2 were obtained for alkyl chains).

Rather long relaxation runs were carried out for all the configurations by holding the two lowermost Si layers fixed at the bulk Si lattice positions and allowing all the other Si and H atoms, and the SNP molecule as well, to be free to relax. After about 100 relaxation steps, the absolute atomic displacements for all the configurations are below 0.001 Å/step, while the forces are converged to the conventional figure of $\leq 10^{-3}$ eV/Å. In the case of the double-bond configuration (3), a similar run was carried out also for the 12-layer supercell, containing 71 atoms, starting from the already relaxed monolayer-surface configuration of the eight-layer simulation, without finding any qualitative difference.

We calculate total energy differences between the various configurations involved where necessary by adjusting H stoichiometry. $E_H = -12.959$ eV is the total energy of a free hydrogen atom in our LDA pseudopotential scheme, which underestimates the experimental value by about 5%. Because this value is affected by a large uncertainty, the following results (see also Figure 7) are given by explicitly separating the E_H contribution, so as to allow comparison with results obtained by different pseudopotential schemes.

The single-bond, fully reduced surface configuration (1) is found to be the lowest in energy, having a $\Delta E - 2E_H = -1.80$ eV lower than the sum of the energies of the separate Si−surface and monolayer subsystems. However, as noted above, its formation requires a suitable H pressure and, moreover, the cleavage of the Si−Si dimer. Indeed, cleavage of the surface dimer of the (2 × 1) Si(100) surface was observed during chemisorption of cyclic hydrocarbons, accompanied by dehydrogenation.[28]

The single-bond, surface-reconstructed configuration (2) is chemically stable, its total energy difference being $\Delta E = -1.31$ eV below the reactants. Such a configuration appears stable also toward the cleavage of the surface dimer, i.e., the unsaturated intermediate state (2′) (Figure 7), which is chemically stable as well, but has a $\Delta E = -0.09$ eV, i.e., higher by +1.22 eV than the (2). The half-saturated intermediate state (2″) is also found to be stable, with $\Delta E - E_H = -0.37$ eV. This configuration could evolve into the (1) upon full reduction by a second H atom. However, such an intermediate state has a zero-energy barrier toward the oversaturated state (1′) (see Figure 7), in which the surface dimer is not broken, but the surface Si is bound to two H atoms. The energy of such an intermediate configuration is $\Delta E - E_H = -1.08$ eV below the reactants.

Finally, the double-bond, dimer-reconstructed configuration (3) is chemically unstable because its energy lies at $\Delta E + 2E_H = +2.80$ eV above the sum of the energies of the reactants.

We note that all the above results alone are not sufficient to determine the surface configuration because the H stoichiometry changes, and moreover, they are all relative to zero temperature. At finite temperatures, the actual interface structure is deter-

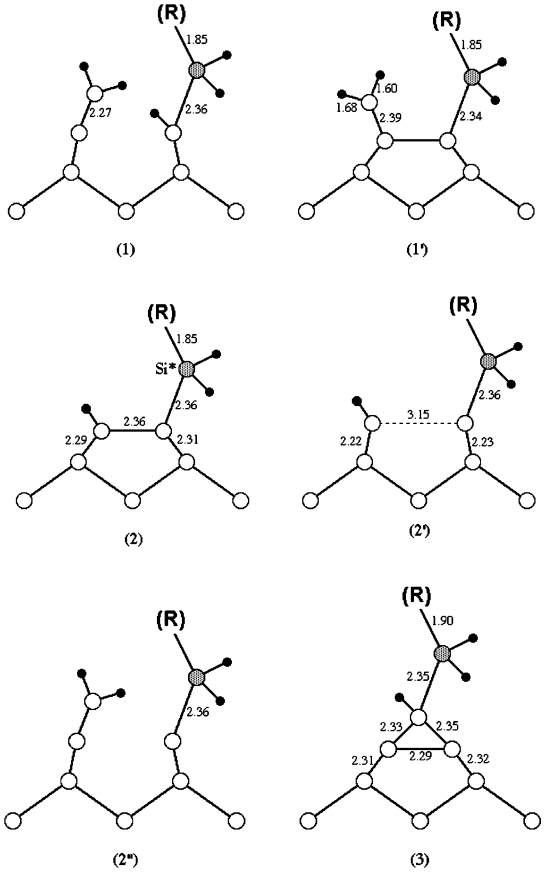

Figure 7. Atomic configurations of the Si(100). SNP interface. The gray-shaded ball is the terminal Si* atom of the SNP molecule, the latter being indicated by (R). Bond lengths are in Ångstroms.

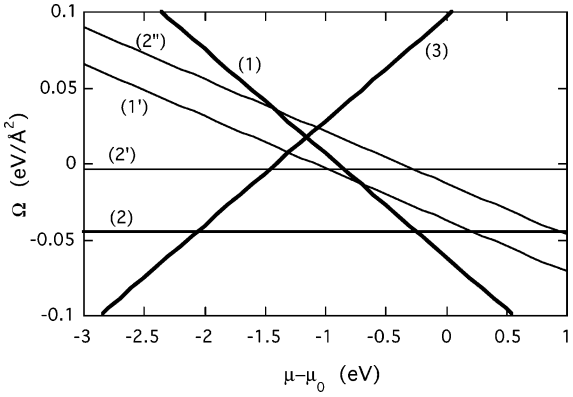

Figure 8. Grand-canonical potential per unit surface area as a function of the H chemical potential, μ_H, of the various interfacial configurations Si−monolayer. See Figure 7 for the indexing of the configurations.

mined by the grand-canonical potential Ω, eq 1, at the fixed value of the SNP molecule chemical potential corresponding to a full monolayer coverage. In Figure 8, we draw a tentative plot of Ω for all the configurations explored in this study. It can be seen that, although unstable at high H chemical potential, the configuration (3) can be the preferred one under very high vacuum, at $\mu < \mu_0 - 2$ eV (note the difference in the scale of μ with respect to Figure 4, and recall the logarithmic relation between μ and P) because it liberates free H. The configuration (2) is the next stable one, up to $\mu = \mu_0 - 0.25$ eV, above which the (1) is stable at any H pressure. At finite temperatures, the entropy contribution will alter this stability diagram, and other configurations could compete with the above ones. In particular, we note the interval $\mu - \mu_0 = -1.3$ to -0.7 eV, in which the Ω for the configurations (2′), (1′), and (1) come very close to each other, meaning that, as a function of increasing H pressure and substrate temperature, H atoms could indeed supersaturate the dimer, possibly cleaving the Si−Si bond, until the configuration (1) is finally stabilized. However, note that configuration (1′), with its largely strained Si−H bonds, instead of evolving to the (1) could rather be a prelude to the desorption of a H_2 molecule, as it was found in accurate quantum-chemical calculations of hydrogen desorption from Si surfaces.[29]

B. Interface Bonding Structure. The configuration (1) (Figure 6a, see also Figure 7 for the bond lengths) ends up with the Si*−Si bond (the "*" indicating the terminal Si of the SNP molecule) being stretched to 2.36 Å, while the surface Si−Si bonds are in the range 2.31−2.32 Å. The Si−H_2 surface group exhibits a strong relaxation by tilting as a whole by about 45°, the corresponding Si−Si bond length being contracted to 2.27 Å. Such a behavior is reminiscent of the tilting observed in the (2 × 1) reconstruction of the Si(100) surface (Figure 3f), moreover enhanced by the depressed electron density region created at the surface by the long Si*−Si bond. By comparison, in the configuration (2) (Figure 6b), the Si*−Si bond is 2.36 Å and the Si*−C is 1.85 Å, as in (1). The Si−Si dimer is 2.36 Å, while the Si−Si bonds in the first and second surface layer are in the range 2.29−2.32 Å. Finally, the configuration (3) (Figure 6c) ends up with Si*−Si bond lengths in the range 2.33−2.35 Å; similar to the configuration (2), the Si−Si bonds in the first and second surface layer are contracted to 2.29−2.32 Å, the surface dimer having, however, the smallest value. The Si*−C bond length in the terminal part of the SNP molecule is 1.90 Å, i.e., 3% longer than in the free molecule.

Notably, the bond angles appear much closer to the ideal tetrahedral coordination in the configurations (1) and (2), than in the (3), in which the Si−Si*−Si structure is constrained to an isosceles triangle. In fact, in (3), the tetrahedron centered on the Si* atom, formed by C−H−Si−Si, has only one $A\hat{B}C$ angle of 107°, close to the regular tetrahedral value of 109.4°, while all the others are either much smaller or much larger, going from 98° to 145°. The average length of the tetrahedron edges is 3.27 ± 0.47 Å. On the other hand, for the corresponding Si*-centered tetrahedron in (1), formed by C−H−H−Si, all the angles are comprised between 104° and 116°, the average edge length is 3.00 ± 0.15 Å. Overall, the latter results an almost regular tetrahedron. The configuration (2) has a somewhat intermediate structure, with all the Si*−Si−Si−Si tetrahedron angles around 105−108°, but one value of 122° for the angle between the Si* and the surface dimer; the average edge length is in this case 3.90 Å, with a relatively small dispersion of ±0.15 Å. From a structural point of view, such results together with the data on the bond lengths make the single-bond configurations (1) and (2) the preferred ones.

C. Electronic Structure. In Figure 9, we represent the LDOS projected on the Si slab, on the alkyl chain (C_σ), and the phenyl head (C_π) of the SNP molecule, for the three bonding configurations (top panel for the (1), middle for the (2), bottom for the (3)). The fragment of the molecule corresponding to the double-oxygen bridge is included in C_π, while the Si* is included in C_σ. The Fermi level, or the top of the valence band for intrinsic Si, is at $E_F = +0.05$ eV for all the configurations.

The LDOS for the configuration (1) shows that contacting the SNP monolayer to the Si substrate has further blue-shifted the whole molecular spectrum, the π HOMO being now located at $E_H = -1.35$ eV, and the π^* LUMO at $E_L = +3.18$ eV. The amplitude of the gap is therefore 4.53 eV, slightly larger than the free-standing monolayer, and slightly smaller than the gas-

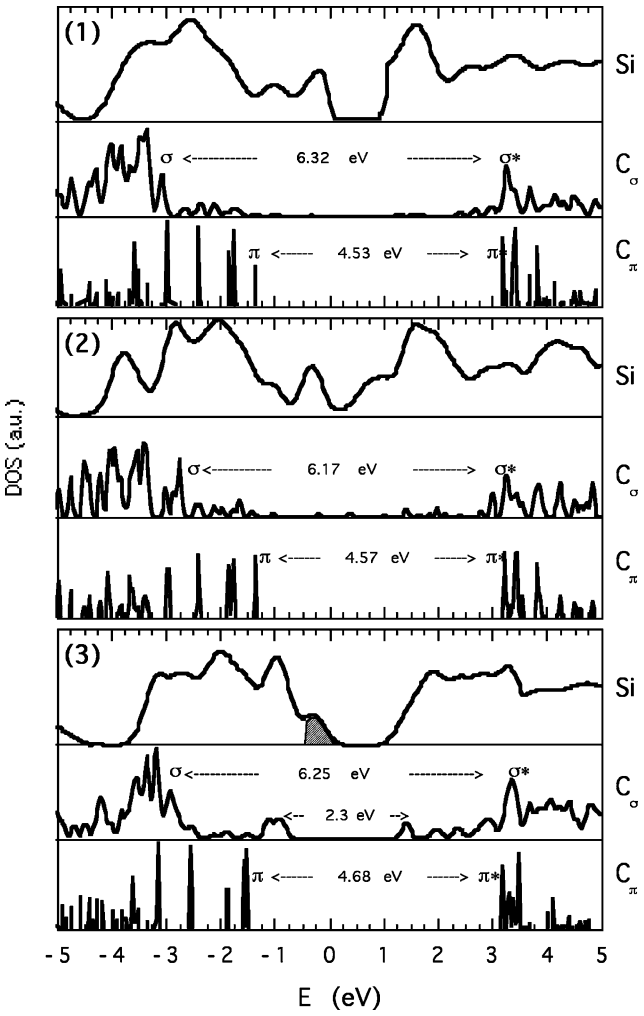

Figure 9. LDOS for the configurations (1), (2), and (3) of the Si−SNP interface. Si: bulk Si slab, C_σ = alkyl chain of the SNP monolayer, C_π = phenyl head of the SNP monolayer. The common Fermi level is shifted at $E_F = 0$.

phase molecule value. The $\sigma-\sigma^*$ gap, equal to 6.32 eV, still lies well outside the $\pi-\pi^*$ gap. Similar to the free molecule and free monolayer spectra, the σ^* is very close to the π^*, nearly forming a single band. However, we note that the HOMO level is *not* aligned, or even close, to the Fermi level of the substrate, at variance with the assumptions of some recent molecular electronics studies.[5] This could be the signature of nonalignment of the respective vacuum levels, hampered by the formation of a dipole layer at the Si−SNP interface. In fact, by performing a simple Hirshfelder analysis of the charge around each atom, and by subtracting the values for the separate Si surface and free monolayer, we find that a negative charge of about $-0.035e$ is accumulated around the surface Si atom bound to the Si*. We note that some negative charge accumulates around the Si* as well, but this is neutralized by a corresponding positive charge increase in the two nearby H atoms. Therefore, assuming an equal amount of positive charge in the surface layer between Si and Si*, this would give rise to a local dipole of ∼0.2 D, or a surface dipole of about 7×10^{-3} Debye/Å^2, directed away from the Si surface.

The monolayer energy spectrum is practically unchanged in configuration (2) (Figure 9, center). However, the bulk Si LDOS clearly shows a reminder of the (2×1) monohydride Si(100) surface LDOS. The gap is almost completely filled by a band that is only partly ascribable to the surface layers, being shared also with lower-lying Si layers. Also, in this case, such an effect can be traced back to the straining of the back-bonds connecting the surface layers to the bulk Si.

The bonding configuration (3) is found to be unfavorable with respect to the (1) and (2), also on the basis of the LDOS analysis (Figure 9, bottom panel). We see a first peak in the Si LDOS immediately below the Fermi level, at $E = E_F - 0.22$ eV, originating from states localized at the Si(100) surface (shaded area in Figure 9). The energy level spectrum of the SNP monolayer is strongly influenced and rearranged as a consequence of the peculiar bridge-like Si*−Si−Si bonding of this configuration. Both the HOMO and LUMO are spurious σ-like bands, localized in the portion of the alkyl chain closer to the interface with Si. They appear to be induced within the original $\pi-\pi^*$ gap by the bridge-like bond. Notably, the HOMO is aligned at $E = E_F - 0.89$ eV, with the *second* peak below the Fermi energy ($E_F = +0.05$ eV, coincides with the top of VB), i.e., the first peak strictly composed by Si surface states is skipped. The first unoccupied (LUMO) molecular orbital above E_F is almost lined up with the Si CB bottom; a LUMO + 1 orbital is located at $E = E_F + 2.86$ eV. Both bands have σ^* character. Notably, the two nearest $\pi-\pi^*$ bands around E_F are the peaks centered at $E = E_F - 1.53$ eV and $E = E_F + 3.18$ eV (a shoulder of the peak centered at $E = E_F + 3.33$ eV), i.e., the actual $\pi-\pi^*$ gap is about ∼4.7 eV, larger than both the free molecule value and that of the dense monolayer.

5. Conclusions

In this work, we have studied, by means of DFT-LDA calculations, the atomic and electronic structure of several different interfaces between the Si(100) surface and a dense monolayer of a model molecule composed by a long alkyl chain and a phenyl head. It was our aim to characterize a representative organic−inorganic semiconductor interface of the type already employed in the synthesis of molecular electronics devices.[5]

In the free-standing monolayer, we have found evidence for a strong effect of intermolecular screening of the electrostatic interaction. The major result of such a screening, already observed experimentally in several organic−inorganic interfacial systems,[13,16,17] is the reduction of the ionization potential and electron affinity so as to render the conductivity gap close to the HOMO−LUMO gap.

Concerning the chemisorption of the monolayer onto the (2×1) dimerized Si(100) surface, we studied three different bonding configurations and characterized their relative chemical stability as a function of the available H pressure. The analysis of the electronic structure of the Si−monolayer interfaces reveals that only the fully H-reduced interface with cleaved Si−Si surface dimer presents a clean semiconductor gap in the Si side and a minimal perturbation of the monolayer energy level spectrum. In the other interfaces, which maintain the Si−Si surface dimer, surface-localized states are always induced in the Si gap. Such localized states are likely to alter the electronic characteristics of the molecular device by creating a substantial contact resistance. In the case of the bridge-like interface, in which the molecule sits in the middle of the Si−Si dimer, bonded to both Si atoms, the monolayer spectrum is strongly perturbed, and spurious states with $\sigma-\sigma^*$ character appear within the pristine HOMO−LUMO gap, mostly localized in the terminal fragment of the molecule closer to the Si surface.

In all the above interfacial systems, we find that the HOMO of the monolayer does not align with the Fermi level of the Si substrate, but rather it is shifted by about −1.3 eV below it. Such a behavior is correlated with the appearance of an interface dipole, originated by the accumulation of negative charge in

the Si surface first layer. This should be the manifestation of a nonalignment of the vacuum level between the organic and inorganic semiconductor, as already found in experimental studies on different organic−inorganic couples.[30] Such a latter issue is currently under study and will be more thoroughly discussed in a forthcoming paper.

6. Computational Details

All the results have been obtained with the ABINIT, plane-wave density functional theory (DFT) code.[31] Local-density approximation (LDA) was used together with pseudopotentials to describe core electrons. Different pseudopotential schemes were tested (standard Troullier−Martins,[32] Teter-extended norm-conserving,[33] HGH dual-space double-Gaussian[34]), with the restriction that all the elements in a simulation must share the same cutoff of the plane-wave expansion and the same exchange-correlation functional. The best compromise was obtained with the Troullier−Martins for all the elements but hydrogen, written in the Kleinmann−Bylander separable form, and using the Ceperley−Alder LDA functional.[35] For H, a bare Coulomb-core unscreened potential was used. The common kinetic energy plane-wave cutoff was set at 680 eV.

Most free-molecule and monolayer calculations were carried out with a fictitious Gaussian smearing of the electron density with a convergence parameter of 0.01 Ha. Anderson mixing of electron densities was generally found to improve the convergence rate. Structural relaxation was carried out by a modified Broyden−Fletcher algorithm, and damped molecular dynamics was used in some cases to explore competing minima.

The local electronic density of states (LDOS) is inferred by performing an atom-by-atom projection of the charge density. In practice, a sphere of radius $R = 3.2$ b ($\sim$1.7 Å) is drawn around each atom so as to include eventually the H atom nearby, and the total charge density for each eigenvalue is calculated by spherical harmonics projection operators, summed over the different angular momentum quantum numbers. Such partial charges are then normalized and used as fractional weights in the calculation of the Gaussian-smoothed DOS, which can be summed up into different portions: the Si(100) slab, the σ chain, and the π-head fragment of the SNP molecule, respectively.

Acknowledgment. F.C. thanks the Section de Mathématique et Physique of the CNRS for a scholarship grant to visit the IEMN in Villeneuve d'Ascq. Work of F.C. and S.L. was supported by the ENEA-MIUR project L.295/1997 TANO "Tecnologie e Applicazioni della Nanoorganica in Microelettronica".

References and Notes

(1) Joachim, C.; Gimzewski, J. K.; Aviram, A. *Nature* **2000**, *408*, 541.
(2) Delamarche, E.; Michel, B.; Byebuick, H. A.; Gerber, C. *Adv. Mater.* **1996**, *8*, 719.
(3) See, e.g.: Ulman, A. *Ultrathin Organic Films*; Academic Press: New York, 1991.
(4) Boulas, C.; Davidovits, J. V.; Rondelez, F.; Vuillaume, D. *Phys. Rev. Lett.* **1996**, *76*, 4797.
(5) Lenfant, S.; Krzeminski, C.; Delerue, C.; Allan, G.; Vuillaume, D. *Nano Lett.* **2003**, *3*, 741.
(6) Mui, C.; Bent, S. F.; Musgrave, C. B. *J. Phys. Chem. A* **2000**, *104*, 2457.
(7) Luo, H.; Lin, M. C. *Chem. Phys. Lett.* **2001**, *343*, 219.
(8) Seino, K.; Schmidt, W. G.; Furthmuller, J.; Bechstedt, F. *Phys. Rev. B* **2002**, *66*, 235323.
(9) Parikh, A. N.; Allara, D. L.; Azouz, I. B.; Rondelez, F. J. *J. Phys. Chem.* **1994**, *98*, 7577.
(10) Burrow, P. D.; Michejda, J. A.; Jordan, K. D. *J. Chem. Phys.* **1986**, *86*, 9.
(11) Tobik, J.; Del Corso, A.; Scandolo, S.; Tosatti, E. *Surf. Sci.* **2004**, *566−568*, 644.
(12) Veenstra, S. C.; Jonkman, H. T. *J. Polym. Sci., Part B: Polym. Phys.* **2003**, *41*, 2549.
(13) Harder, E.; Kim, B.; Friesner, R. A.; Berne, B. J. *J. Chem. Theory Comput.* **2005**, *1*, 169.
(14) Makov, G.; Payne, M. *Phys. Rev. B* **1995**, *51*, 4014.
(15) Rotenberg, E.; Enkvist, C.; Brühwiler, P. A.; Maxwell, A. J.; Mårtensson, N. *Phys. Rev. B* **1996**, *54*, R5279.
(16) Wang, L. S.; Conceicao, J.; Jin, C.; Smalley, R. E. *Chem. Phys. Lett.* **1991**, *82*, 5.
(17) Ishii, H.; Sugiyama, K.; Ito, E.; Seki, K. *Adv. Mater.* **1999**, *11*, 605.
(18) Dabrowski, J.; Scheffler, M. *Appl. Surf. Sci.* **1992**, *56*, 15.
(19) Jung, Y.; Shao, Y.; Gordon, M. S.; Doren, D. J.; Head-Gordon, M. *J. Chem. Phys.* **2003**, *119*, 10917.
(20) Shkrebtii, A. I.; Di Felice, R.; Bertoni, C. M.; Del Sole, R. *Phys. Rev. B* **1995**, *51*, R11201.
(21) Rohlfing, M.; Krüger, P.; Pollmann, J. *Phys. Rev. B* **1995**, *52*, 13753.
(22) Sakurai, T.; Hagstrum, H. D. *Phys. Rev. B* **1976**, *14*, 1593.
(23) Chabal, Y. J.; Ragavachari, K. *Phys. Rev. Lett.* **1985**, *54*, 1055.
(24) Northrup, J. E. *Phys. Rev. B* **1991**, *44*, 1419.
(25) Dubois, M.; Perdigão, L.; Delerue, C.; Allan, G.; Grandidier, B.; Deresmes, D.; Stiévenard, D. *Phys. Rev. B* **2005**, *71*, 165322.
(26) Kaganer, V. M.; Möhwald, H.; Dutta, P. *Rev. Mod. Phys.* **1999**, *71*, 779.
(27) May, S.; Kozlovsky, Y.; Ben-Shaul, A.; Kozlov, M. M. *Eur. Phys. J. E* **2004**, *14*, 299.
(28) Kong, M. J.; Teplyakov, A. V.; Jagmohan, J.; Lyubovitsky, J. G.; Mui, C.; Bent, S. F. *J. Phys. Chem. B* **2000**, *104*, 3000.
(29) Pai, S.; Doren, D. *J. Chem. Phys.* **1995**, *103*, 1232.
(30) Chassé, T.; Wu, C.-I.; Hill, I. G.; Kahn, A. *J. Appl. Phys.* **1999**, *85*, 6589.
(31) The ABINIT code is a common project of the Université Catholique de Louvain, Corning Incorporated, and other contributors. See: Gonze, X.; Beuken, J.-M.; Caracas, R.; Detraux, F.; Fuchs, M.; Rignanese, G.-M.; Sindic, L.; Verstraete, M.; Zerah, G.; Jollet, F.; Torrent, M.; Roy, A.; Mikami, M.; Ghosez, Ph.; Raty, J.-Y.; Allan, D. C. *Comput. Mater. Sci.* **2002**, *25*, 478.
(32) Troullier, N.; Martins, J. L. *Phys. Rev. B* **1991**, *43*, 1993.
(33) Teter, M. *Phys. Rev. B* **1993**, *48*, 5031.
(34) Hartwigsen, C.; Goedecker, S.; Hutter, J. *Phys. Rev. B* **1998**, *58*, 3641.
(35) Ceperley, D.; Alder, B. J. *Phys. Rev. Lett.* **1980**, *45*, 566.